A Supercritical Lens Optical Label-Free Microscopy: Sub-Diffraction Resolution and Ultra-Long Working Distance

*Fei Qin, Kun Huang, Jianfeng Wu, Jinghua Teng, Cheng-Wei Qiu, and Minghui Hong**

The optical microscope is widely employed in both scientific researches and industrial communities. Its resolving power is limited by the Rayleigh diffraction limit 0.61λ/NA (where NA is numerical aperture), even for the ideal optical system without any imperfection or aberration.[1] During the past decades, great efforts have been devoted to breaking the diffraction limit, which could be categorized into near-field and far-field operations in general. The near-field approaches, such as superlens,[2,3] hyperlens,[4,5] microsphere assist imaging,[6,7] and near-field scanning optical microscopy,[8] use the evanescent waves containing high spatial frequencies to solve fine objects. So the imaging process needs to be performed very close to the sample, which brings significant challenges in practical applications. Stimulated emission depletion microscopy (STED), photo-activated localization microscopy (PALM), and stochastic optical reconstruction microscopy (STORM) are able to provide the resolution at tens of nanometer in far-field by selectively activating or deactivating fluorophores.[9–11] However, the preprocessing and labeling of samples by specific dyes make these techniques only valid for imaging biology specimen.

Recently, a non-invasive universal imaging technique, called as super-oscillatory lens (SOL) optical microscopy, was invented. This technology provides a promising way to achieve pure optical super-resolution imaging in far-field, could be used at any wavelength, and does not depend on the luminescence of object. However, it is still struggling against several intractable issues:[12–17] (i) image distortion and small field of view caused by the inevitable side-lobes of a super-oscillatory spot; (ii) complicated nano-lithographic technique required in fabrication due to the sub-wavelength features sizes; (iii) short working distance leading to a low tolerance of optical misalignment and environmental disturbance; (iv) short depth of focus (DOF), then consequently, a tiny bit of deviation in the object position resulting in huge degradation of super-resolution property. To surmount these inherent barriers and bring the academic concept into practical applications is always a big challenge.[18] The far-field sub-wavelength focusing has also been demonstrated by other nano-structured lenses, such as photon nanosieve meta-lens and graphene oxide flat meta-lens, which unfortunately suffer from similar problems like SOL.[19,20] Furthermore, although a sub-wavelength optical needle can be obtained by focusing the radially polarized (RP) beam, its undetectable longitudinal component by the usual optical system severely limits its applications.[21,22]

In this Communication, we propose a non-invasive microscopy based on a concept of supercritical lens (SCL), and experimentally recognize a pattern with the minimal feature size of 65 nm (0.16λ) in air under the illumination wavelength of 405 nm. This microscopy exhibits an ultra-long working distance of 55 μm (135λ), one order improvement compared to the reported SOL results, providing sufficient space for samples' adjustment. The focusing spot of such lens has a lateral width of 0.407λ without significant side-lobes, and shows an $\approx 12\lambda$ needle-like focal region along the light propagation, ensuring high tolerance in axial positioning. All these benefits enable us to achieve a high-quality image for a large-area object at a high scanning speed. Our SCL microscopy makes the first attempt to map the horizontal detail of a 3D object, which significantly extends the scope to the regimes that are unexploited in other microscopies.

For a planar diffraction lens, the lateral size and axial position of its focal spot, in principle, can be customized by optimizing the lens (i.e., width and radial position of each belt). The traditional Fresnel zone plate (FZP) usually focuses light into an Airy spot of $|J_0(kr\mathrm{NA}) + J_2(kr\mathrm{NA})|^2$ with the size of 0.61λ/NA, which is the same as the Rayleigh criterion (RC) defined in the spherical-lens-based optical imaging system,[23] accompanied by a very weak side-lobe with a mere 1.75% intensity of main spot. Sub-diffraction limit focusing is feasible but needs to pay the cost of the increasing side-lobes. Adjusting the proportion of high and low spatial frequencies should be elaborately considered in the optimization, because the light with higher spatial frequencies corresponds to a smaller main spot. The extreme case is that, light with only the maximum spatial frequency is focused into a hotspot of $|J_0(kr\mathrm{NA})|^2$, which is named as maximum-frequency spot,[24] where J_0 is the zero-order Bessel function of the first kind, r is the radial position in polar coordinates, $k = 2\pi/\lambda$ and λ is the wavelength, as shown in **Figure 1**a. This maximum-frequency spot has a main-lobe of 0.38λ/NA and comes with moderate side-lobes. The peak-intensity ratio between the strongest side-lobe and central main-lobe is 16.2%, which is usually acceptable in practical applications. The DOF could be extended into a needle-like focal region while the main-lobe size is slightly larger than 0.38λ/NA. The focal spot certainly can be further reduced so that the light in the main-lobe region oscillates faster than the

Dr. F. Qin, Dr. J. Wu, Prof. C.-W. Qiu, Prof. M. Hong
Department of Electrical and Computer Engineering
National University of Singapore
4 Engineering Drive 3, Singapore 117583, Singapore
E-mail: elehmh@nus.edu.sg
Dr. K. Huang, Dr. J. Teng
Institute of Materials Research and Engineering
Agency for Science Technology and Research (A*STAR)
2 Fusionopolis Way, Innovis, #08-03, Singapore 138634, Singapore
Dr. J. Wu
Department of Physics
National University of Singapore
2 Science Drive 3, Singapore 117542, Singapore

DOI: 10.1002/adma.201602721

© 2016 WILEY-VCH Verlag GmbH & Co. KGaA, Weinheim

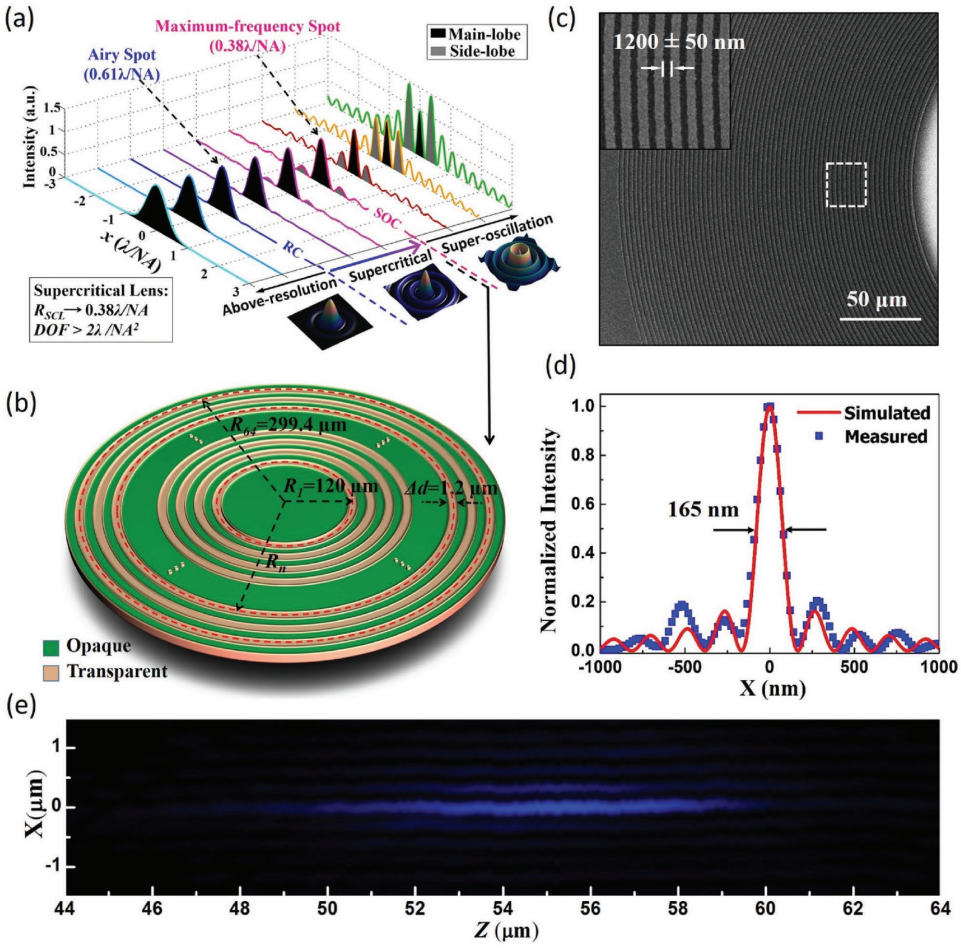

Figure 1. Design and characterization of the supercritical lens. a) Possible intensity patterns of focal spots by planar lens. By Rayleigh criterion (RC) and super-oscillation criterion (SOC), the focal spots are categorized into three gradually variant ranges. From the range of above-resolution to super-oscillation, the size of main-lobe decreases smoothly, accompanied by the gradually increasing side-lobes, as the inset field patterns shown. R_{SCL}: Radius of supercritical hotspot. b) Schematic configuration of the 405 nm supercritical lens. R_n represents the radius of the central circle (dashed) in the nth belt, and the width Δd is fixed at 1.2 μm for all belts. c) SEM image of the fabricated supercritical lens. The zoom-in view of the dashed box is shown in the upper-left corner. d) Comparison of the line intensity profiles along x-axis of the focal spot between the simulated and experimental results. e) Measured intensity profile of the optical needle along the propagation distance in the region from z = 44 to 64 μm.

maximum-frequency hotspot, which is termed as super-oscillation in mathematics.[25] Correspondingly, $0.38\lambda/NA$ kept in maximum-frequency spot is taken as super-oscillation criterion (SOC).[24,26] However, the cost is that the side-lobe intensity increases exponentially, and the depth of focus is extremely short, which imposes a big challenge on its applications, although it holds the promise for an infinitesimal main spot.[13]

The terminology of supercritical is usually used to describe a physical state above a critical threshold, leading to some intriguing properties, such as supercritical fluid in condensed matter physics, supercritical aerofoil in aerodynamics field, supercritical mass in nuclear physics, etc. From the above analyses, it is found that the sub-diffraction limit focal spot with a long DOF could be achieved when the optimization target is set in the range from RC to SOC. To emphasize this point, as depicted in Figure 1a, we define the SCL as a planar diffraction component which has a focusing spot slightly larger than SOC (0.38λ/NA), and a needle-like focal region with its DOF $\Delta z > 2\lambda/\mathrm{NA}^2$ that differs from traditional spherical lens, FZP, SOL, and others.[23] The threshold in our case is the super-oscillation criterion, and the unique properties are its sub-diffraction-limited focal spot, weak side-lobe, ultra-long focal length, and needle-like focal region.

Figure 1b presents the sketch of the 405 nm SCL composed of a series of concentric transparent belts. The focal length of this SCL is chosen at $z = 135\lambda$ for a large operation space in subsequent imaging process. Distinguished from SOL with destructive interference, our SCL employs the constructive interference, which allows more light with high spatial frequencies to obtain the required sub-wavelength needle light. Therefore, through tuning the positions of each belt, the designed lens has 64 transparent belts with the largest radius R_{64} = 299.4 μm, and the smallest radius R_1 = 120 μm which filters out the lower spatial frequencies of light. All the belts have a fixed non-sub-wavelength width Δd = 1.2 μm for facile fabrication, and the smallest gap between two neighboring belts is 1.4 μm, also in

© 2016 WILEY-VCH Verlag GmbH & Co. KGaA, Weinheim

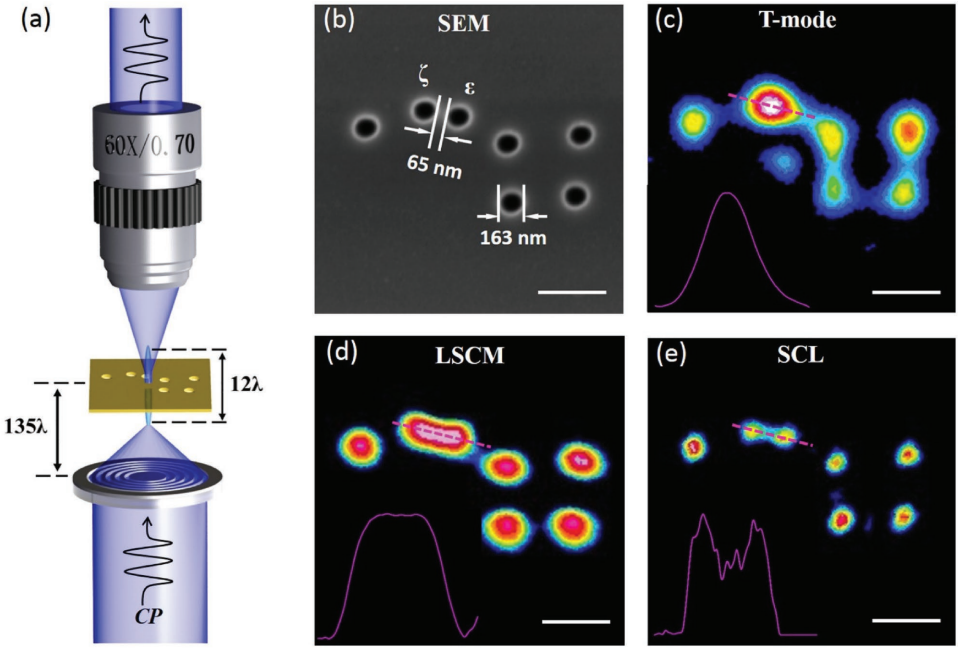

Figure 2. Super-resolution imaging of SCL microscopy. a) Schematic of SCL microscopy. When the SCL is illuminated by a 405 nm circular polarized (CP) beam, a sub-wavelength optical needle with 12λ long is formed at 135λ away from the SCL plane. The imaging sample is placed in the needle range and raster scanning in x-y plane. The transmitted signal is collected by an objective. b) SEM of nanoscale Big Dipper used for the resolution demonstration. c) Imaging result by a normal transmission-mode (T-mode) microscope with an NA = 0.9 objective lens under the illumination of 405 nm wavelength. d) Imaging result by the laser scanning confocal microscopy (LSCM) with the same wavelength and objective lens. For the better comparison, LSCM image is presented with inverted color from the source image, since the LSCM is working in reflection mode which differs from others. e) Imaging result by SCL microscopy which shows that the 65 nm space between the stars ε and ζ can be clearly distinguished. These images are presented by pseudo-color for a better view. Insets are the line intensity profiles through the center of stars ε and ζ for each image. Scale bars: 500 nm.

non-sub-wavelength scale. By utilizing the conventional laser pattern generator, we patterned the SCL directly on a standard chrome photo-plate by precisely controlling the parameters of the fabrication process (see the Supporting Information for more details about the design and fabrication of SCL). The scanning electron microscopy (SEM) image of the fabricated SCL, as shown in Figure 1c, indicates that the fabrication error can be controlled under ±50 nm to guarantee the focusing performance of SCL without significant deviation. The optical image of the entire SCL is shown in Figure S1 (Supporting Information). In order to characterize its focusing properties, a 405 nm wavelength circular polarized beam is used to illuminate the SCL from the substrate side. A focal spot with its full-width-half-maximum (FWHM) of 165 nm (0.407λ) in lateral size is experimentally obtained at a distance of 55 µm (≈135λ) away from the SCL. The line intensity profiles of the focal spot are plotted in Figure 1d, which witnesses excellent agreement between the simulated and measured results. A 3D view of the measured intensity profile shows that the intensity pattern is dominated by the central main-spot without significant side-lobes (see Figure S2, Supporting Information). Moreover, as depicted in Figure 1e, the focal spot could stably maintain and form the required needle-like focal region from z = 53 to 58 µm in experiment, which would greatly benefit the imaging performance.

Based on the SCL, a customized microscope system working in scanning scheme was built for the demonstration of super-resolution imaging. The imaging sample is placed at the focal region of SCL, and scanned in x-y plane by a piezo-stage during the imaging process, as illustrated in **Figure 2**a for the working principle. The light scattered from the object is collected by an objective lens and finally projected onto a photomultiplier tube (PMT). For its further details and image of the real apparatus, see Figure S3 (Supporting Information). In order to filter out the halo effect caused by the side-lobes, a 10 µm diameter pinhole is employed and placed at the position that is conjugated with the object plane. In fact, the pinhole can also slightly improve the imaging resolution of the whole system, but it is more desired to enhance the imaging contrast in terms of eliminating the halos beyond the central spot region (see Figure S4, Supporting Information). In addition, working as a purely focusing element in such a scanning scheme, our SCL is able to avoid the complicated aberration correction that must be involved for the high-quality imaging in a conventional projection scheme.

To demonstrate its resolving capability, we use the SCL microscope to image a nanoscale Big Dipper with stars taken as nanoholes with 163 nm diameter in average, which are fabricated on a 100 nm thick chromium film by focused ion beam (FIB) milling. As the SEM image shown in Figure 2b, the smallest gap between stars ε and ζ is only 65 nm, which is far beyond the diffraction limit for visible light. When this pattern is examined by a conventional microscope with a NA 0.9 objective in transmission-mode (T-mode), the signal of stars ε and ζ are mapped into a blob, and cannot be resolved at all (Figure 2c). Whereas the 405 nm wavelength

© 2016 WILEY-VCH Verlag GmbH & Co. KGaA, Weinheim

laser scanning confocal microscopy (LSCM) also fails to resolve them (Figure 2d). In comparison, our SCL microscopy reveals all fine topology of the nanoscale Big Dipper, including the stars ε and ζ with 65 nm gap in between (Figure 2e). In addition, the reconstructed image by our SCL-based system shows decent contrast performance, saving any further modification or image post-processing (see the Supporting Information for movie of the scanning process). The line profiles through the center of stars ε and ζ for each image are depicted in the insets of Figure 2c–e, which evidences the dramatic improvement of the SCL imaging resolution. Moreover, as shown in the inset of Figure 2e, the contrast between the peak and valley of the SCL profile is around 30%–40%, which is larger than 20% defined in Rayleigh resolving criterion for distinguishing two neighboring points in an image.[1] It means that the real resolving ability of our system should be even better than 65 nm. The reconstructed images of the 163 nm diameter holes also show that our SCL microscopy could achieve a high-quality image and reveal the objects with smaller distortion than other techniques. It is worth mentioning that, besides the gap size,[13,27,28] the point spread function (PSF) convolution is also another frequently used methodology to evaluate the resolving power of an imaging system.[29–32] Based on the procedure proposed by Allen et al. in refs. [30] and [32], we performed the image fitting by PSF convolution method. Adopting the Gaussian PSF with a FWHM of $\approx\lambda/3.3$, the fitted image matches well with the experimental one of our SCL microscopy. Therefore, it is the first far-field microscopy that has such resolving capability in air without any pre-processing of samples.

Imaging a large-size object is usually limited by an inevitable obliquity between the sample and lens plane, which leads to the out-of-focus of samples and therefore limits the field of view for an imaging system with a short DOF. To test the capability, the proposed SCL-based system is employed to reconstruct a large-scale non-periodic sample, as shown in **Figure 3**a, which is outlined by several closed curves with the overall footprint of 10×12 μm^2. The imaging results by the T-mode microscopy and LSCM are provided in Figure 3b,c, respectively. Although both microscopies can map the rough contour profiles of the Lion Head, all these fine details are lost. Figure 3d shows the imaging results of our SCL-based system that can clearly distinguish all sophisticated details of this sample. More importantly, all the curves in the entire pattern are shown with nearly equal sharpness, which is mainly attributed to the needle-like focal field with good uniformity of the sub-diffraction limit lateral size in the axial direction (see the Supporting Information for movie of the scanning process).

Another unique advantage of the SCL microscopy is the capability of mapping the horizontal details of a 3D object at one go. **Figure 4**a schematically shows a 3D fishnet wedge composed of transparent holes array surrounding by the opaque background. This fishnet wedge has an oblique angle $\alpha \approx 42.5$ mrad and results in an ≈800 nm height difference between its top and bottom surfaces from left side to right side. The SEM image of the fabricated 3D fishnet wedge is shown in Figure 4b, with 18.8×9.4 μm^2 in size. T-mode microscopy and LSCM can only image the partial object at a certain z-cut plane because their short DOF cannot cover all the holes with different depths, as shown in Figure 4c,d. Therefore, for T-mode microscopy and LSCM, multiple scanning must be performed to reconstruct all the horizontal (x-y plane) details of this 3D object. In contrast, the imaging result by our SCL microscopy presented in Figure 4e shows the clear mapping of this array by precisely addressing the positions of each hole.

It has been long captivated that sub-wavelength imaging requires sub-wavelength features of the lens.[13,20,33,34] The remarkable difference between our SCL with those reported planar lenses is that the smallest feature of our SCL is three times of the working wavelength 405 nm. This translates to the possibility of using conventional laser pattern fabrication

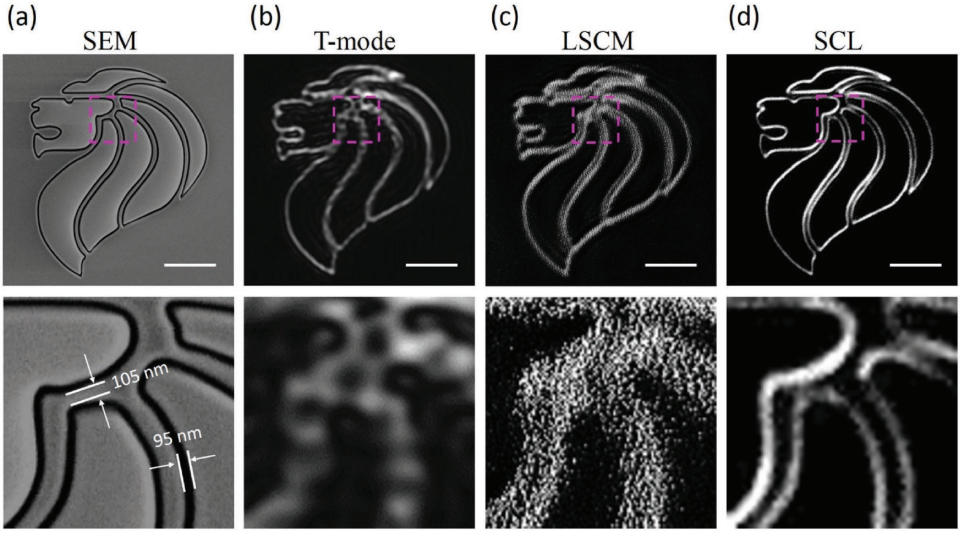

Figure 3. Imaging of a large-scale non-periodic pattern. a) SEM image of a fabricated Lion Head with the overall footprint of 10×12 μm^2. The size of displayed region is 13.5×13.5 μm^2. b–d) Imaging results by transmission mode microscopy (T-mode), laser scanning confocal microscopy (LSCM), and SCL microscopy. The pictures in the upper row are the whole images, and the corresponding zoom-in views of the dashed boxes are shown in the lower row. Scale bar: 3 μm.

© 2016 WILEY-VCH Verlag GmbH & Co. KGaA, Weinheim

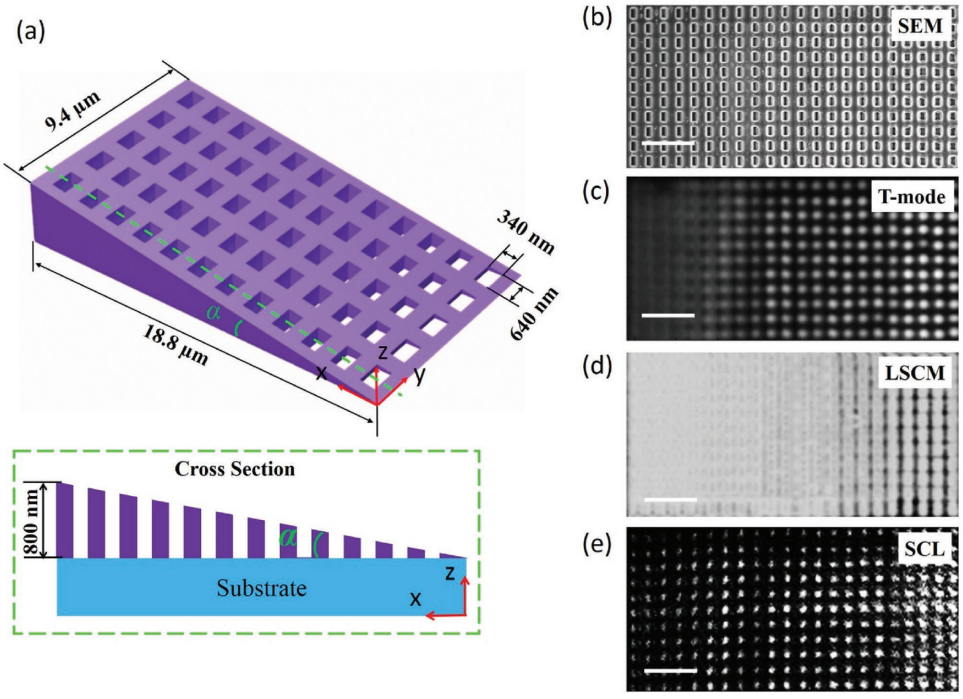

Figure 4. Mapping the horizontal details of a 3D object. a) Sketch of a 3D fishnet wedge composed of an etched array of rectangular holes with the size of 340 × 640 nm^2. Inset: *x*-*z* plane cross section of the fishnet wedge. b) Top-view (*x*-*y* plane) SEM image of the fishnet wedge with a size of 18.8 × 9.4 μm^2. c–e) The imaging results of this wedge by transmission mode microscopy (T-mode), laser scanning confocal microscopy (LSCM), and SCL microscopy. Scale bar: 3 μm.

techniques to make the large-scale lens with high NA, which essentially leads to the deep-sub-wavelength imaging resolution and ultra-long working distance simultaneously. Furthermore, we define a figure of merit FoM = $(s/\delta)^{-1}$, which could be the evaluation indicator of "return on investment (ROI)" for the super-resolution imaging devices, where s is the achieved imaging resolution and δ denotes the smallest feature size of lens that stands for the difficulty level of the lens fabrication. Larger FoM means a higher yield. Our SCL microscopy has the FoM value of ≈18.5, which is enhanced by one order in comparison to ≈1.9 of the previous SOL microscopy.[13]

Another distinct property of our SCL imaging system is the high-speed image reconstruction process. The image with 65 536 pixels, as shown in Figure 2e, is acquired within 794 s by our SCL imaging system (82 px s^{-1}), which is 16 times faster than the reported SOL imaging.[13] Benefiting from this property, we can achieve the large-area scanning without sacrificing the resolution of the reconstructed image in terms of reducing pixel number. Notably, although the PMT possesses much higher quantum efficiency and dynamic range with the response time in the level of nanoseconds, the reconstruction speed is still limited by the low-performance data acquisition (DAQ) card and the long response time of the piezo-stage being used in our current system. If a high-performance DAQ device, such as FPGA (NI, USB-7845R) or other better one, is applied and the working scheme of the piezo-stage is changed from step-by-step mode to continuous scanning mode, the imaging speed can be further increased to 2400 px s^{-1} or even higher (see the Supporting Information for more details, Figure S5, Supporting Information).

In summary, we experimentally demonstrated a SCL optical label-free microscopy which clearly distinguishes a pattern with the minimal feature size of 65 nm in air with a 55 μm working distance. The imaging process is purely physical and captured in real time, does not need any pre-processing to the samples and mathematical post-processing to the imaging results. Such SCL microscopy is able to map the horizontal details of a 3D object at one time scanning, which is impossible for other planar lenses. It overturns a normal captivation that the sub-wavelength imaging requires sub-wavelength features of the lens. This work greatly alleviates those intrinsic problems faced by other planar lenses, and makes the universal super-resolution imaging technique practically applicable. We foresee that the supercritical lens microscopy would open a road for mass production of the high-performance and cost-effective nano-imaging and nano-fabrication technologies.

Supporting Information

Supporting Information is available from the Wiley Online Library or from the author.

Acknowledgements

F.Q., K.H., and J.W. contributed equally to this work. The authors acknowledge Dr. Z. R. Du for the help on sample fabrication. This work was financially supported by National Research Foundation, Prime Minister's Office, Singapore under its Competitive Research Program

© 2016 WILEY-VCH Verlag GmbH & Co. KGaA, Weinheim

(CRP Award No. NRF-CRP10-2012-04) and the A*STAR BEP Grant No. 1521480031.

Received: May 23, 2016
Revised: October 3, 2016
Published online:

[1] M. Born, E. Wolf, *Principles of Optics*, Cambridge University Press, Cambridge **1999**.
[2] X. Zhang, Z. Liu, *Nat. Mater.* **2008**, *7*, 435.
[3] N. Fang, H. Lee, C. Sun, X. Zhang, *Science* **2005**, *308*, 534.
[4] D. Lu, Z. Liu, *Nat. Commun.* **2012**, *3*, 1205.
[5] Z. Liu, H. Lee, Y. Xiong, C. Sun, X. Zhang, *Science* **2007**, *315*, 1686.
[6] Z. Wang, W. Guo, L. Li, B. Luk'yanchuk, A. Khan, Z. Liu, Z. Chen, M. Hong, *Nat. Commun.* **2011**, *2*, 218.
[7] Y. Yan, L. Li, C. Feng, W. Guo, S. Lee, M. Hong, *ACS Nano* **2014**, *8*, 1809.
[8] U. Dürig, D. W. Pohl, F. Rohner, *J. Appl. Phys.* **1986**, *59*, 3318.
[9] K. I. Willig, B. Harke, R. Medda, S. W. Hell, *Nat. Methods* **2007**, *4*, 915.
[10] H. Shroff, C. G. Galbraith, J. A. Galbraith, E. Betzig, *Nat. Methods* **2008**, *5*, 417.
[11] M. J. Rust, M. Bates, X. Zhuang, *Nat. Methods* **2006**, *3*, 793.
[12] M. V. Berry, *J. Phys. A* **2013**, *46*, 205203.
[13] E. T. Rogers, J. Lindberg, T. Roy, S. Savo, J. E. Chad, M. R. Dennis, N. I. Zheludev, *Nat. Mater.* **2012**, *11*, 432.
[14] E. T. F. Rogers, S. Savo, J. Lindberg, T. Roy, M. R. Dennis, N. I. Zheludev, *Appl. Phys. Lett.* **2013**, *102*, 031108.
[15] D. Tang, C. Wang, Z. Zhao, Y. Wang, M. Pu, X. Li, P. Gao, X. Luo, *Laser Photonics Rev.* **2015**, *9*, 713.
[16] C. Wang, D. Tang, Y. Wang, Z. Zhao, J. Wang, M. Pu, Y. Zhang, W. Yan, P. Gao, X. Luo, *Sci. Rep.* **2015**, *5*, 18485.
[17] G. Yuan, E. T. Rogers, T. Roy, G. Adamo, Z. Shen, N. I. Zheludev, *Sci. Rep.* **2014**, *4*, 6333.
[18] T. Taubner, D. Korobkin, Y. Urzhumov, G. Shvets, R. Hillenbrand, *Science* **2006**, *313*, 1595.
[19] K. Huang, H. Liu, F. J. Garcia-Vidal, M. Hong, B. Luk'yanchuk, J. Teng, C.-W. Qiu, *Nat. Commun.* **2015**, *6*, 7059.
[20] X. Zheng, B. Jia, H. Lin, L. Qiu, D. Li, M. Gu, *Nat. Commun.* **2015**, *6*, 8433.
[21] L. Novotny, M. R. Beversluis, K. S. Youngworth, T. G. Brown, *Phys. Rev. Lett.* **2001**, *86*, 5251.
[22] H. Wang, L. Shi, B. Lukyanchuk, C. Sheppard, C. T. Chong, *Nat. Photonics* **2008**, *2*, 501.
[23] L. Novotny, B. Hecht, *Principles of Nano-optics*, Cambridge University Press, Cambridge **2006**.
[24] K. Huang, H. Ye, J. Teng, S. P. Yeo, B. Luk'yanchuk, C.-W. Qiu, *Laser Photonics Rev.* **2014**, *8*, 152.
[25] M. V. Berry, S. Popescu, *J. Phys. A* **2006**, *39*, 6965.
[26] F. Qin, K. Huang, J. Wu, J. Jiao, X. Luo, C. Qiu, M. Hong, *Sci. Rep.* **2015**, *5*, 9977.
[27] M. Khorasaninejad, W. T. Chen, R. C. Devlin, J. Oh, A. Y. Zhu, F. Capasso, *Science* **2016**, *352*, 1190.
[28] H. Yang, R. Trouillon, G. Huszka, M. A. Gijs, *Nano Lett.* **2016**, *16*, 4862.
[29] G. Donnert, J. Keller, R. Medda, M. A. Andrei, S. O. Rizzoli, R. Luhrmann, R. Jahn, C. Eggeling, S. W. Hell, *Proc. Natl. Acad. Sci. USA* **2006**, *103*, 11440.
[30] K. W. Allen, N. Farahi, Y. Li, N. I. Limberopoulos, D. E. Walker Jr., A. M. Urbas, V. N. Astratov, *Opt. Express* **2015**, *23*, 24484.
[31] S. T. Hess, T. P. Girirajan, M. D. Mason, *Biophys. J.* **2006**, *91*, 4258.
[32] K. W. Allen, N. Farahi, Y. Li, N. I. Limberopoulos, D. E. Walker, A. M. Urbas, V. Liberman, V. N. Astratov, *Ann. Phys.* **2015**, *527*, 513.
[33] J. Wang, F. Qin, D. Zhang, D. Li, Y. Wang, X. Shen, T. Yu, J. Teng, *Appl. Phys. Lett.* **2013**, *102*, 061103.
[34] Z. Liu, S. Durant, H. Lee, Y. Pikus, N. Fang, Y. Xiong, C. Sun, X. Zhang, *Nano Lett.* **2007**, *7*, 403.

© 2016 WILEY-VCH Verlag GmbH & Co. KGaA, Weinheim